Available online at www.sciencedirect.com
ScienceDirect
Trans. Nonferrous Met. Soc. China 30(2020) 1300−1314
Transactions of Nonferrous Metals Society of China
www.tnmsc.cn

Tribocorrosion behaviour of Ti6Al4V under various normal loads in phosphate buffered saline solution

R. YAZDI[1], H. M. GHASEMI[1], M. ABEDINI[2], C. WANG[3], A. NEVILLE[3]

1. School of Metallurgy and Materials Engineering, College of Engineering, University of Tehran, Tehran, Iran;
2. Department of Metallurgy and Materials Engineering, Faculty of Engineering, University of Kashan, Kashan, Iran;
3. Institute of Functional Surfaces, School of Mechanical Engineering, University of Leeds, Leeds, LS2 9JT, UK

Received 3 July 2019; accepted 16 February 2020

Abstract: Tribocorrosion tests were conducted on Ti6Al4V against alumina in phosphate buffered saline solution under normal loads of 3−30 N (corresponding to the maximum Hertzian contact pressures of 816−1758 MPa) using a ball-on-disk tribometer. Nano-hardness measurements revealed the formation of work-hardened layers on the pure wear and tribocorrosion surfaces. As the normal load increased from 15 to 30 N during the pure wear, the surface hardness was increased by about 100%. However, a lower generation of wear debris resulted in a lower wear rate under a normal load of 30 N. The presence of corrosion caused an increase in the wear rates by 28%−245% under various normal loads. The corrosion current density acquired from polarization curves was increased by three orders of magnitude and the open circuit potential (OCP) shifted to more negative potentials during tribocorrosion compared with the stagnant condition. The successive formation and removal of tribofilms, which consisted of oxygen and phosphorous compounds, resulted in peaks in the OCP trend and lower fluctuations in coefficient of friction under normal loads higher than 3 N.
Key words: Ti6Al4V alloy; tribocorrosion; nano-hardness; wear; corrosion

1 Introduction

Titanium alloys have a wide variety of applications in medical industries [1,2]. This is due to the formation of a passive film on the surface, which goodly limits the contact between the active metal and body fluid. The passive film results in an excellent corrosion resistance, and prominent biocompatibility [3,4]. However, titanium-based alloys normally possess limitations in wear and tribocorrosion resistance, causing a drawback for use in dynamic contacts [5−7]. Tribocorrosion, as a degradation process, occurs by the combined effect of tribological and corrosive phenomena [8,9]. In tribocorrosion, mechanical damage and corrosive media frequently interact with each other and the results are often different in terms of material removal rates and the mechanisms for either wear and corrosion degradation [10−12]. Indeed, the interaction between wear and corrosion, as indicated by synergy, can change the mechanical, chemical and electrochemical behaviour of materials [10,13]. The synergy can be positive or negative. The surface may be protected by the formation of durable protective layers, i.e., a negative synergy, or suffered from a severer damage than wear alone by excessive material removal, i.e., a positive synergy [14].

Among titanium alloys, Ti6Al4V with alpha−beta structure has the strength to be widely used for metallic joint implants [15]. In artificial joint applications, the dynamic contact between Ti6Al4V and its counterparts may remove the passive layer and expose the bare metal in contact with bio-fluid [16]. Sliding has a detrimental effect

Corresponding author: H. M. GHASEMI; Tel: +98-2161114095; E-mail: hghasemi@ut.ac.ir
DOI: 10.1016/S1003-6326(20)65297-9

on the health by the release of aluminum and vanadium ions in the human body [17]. There have been some reports on tribocorrosion behaviour of titanium alloys in simulated body fluids [18,19]. However, less attention has been paid to the specific role of synergy between wear and corrosion. RUNA et al [18] studied the tribocorrosion induced by the micro-motion between Ti6Al4V stem and bone. They found that the passive film was destroyed during sliding and the presence of protein may act as an obstacle to the formation of a new passive film.

LICAUSI et al [20] worked on the influence of various simulated body fluids on tribocorrosion behaviour of Ti6Al4V. They reported that the tribocorrosion mechanism was wear-dominant; however, it could be changed to corrosion-dominant in acidic medium containing fluorides. In another research [21], Ti6Al4V alloy was fabricated by casting and powder metallurgy, and the effect of fabrication technique on tribocorrosion behaviour was studied. The results represented that the sintered alloy had a better tribocorrosion response for implant applications. It was explained that a more durable tribofilm was formed on the sintered alloy during sliding.

There are various mechanical and dynamic stresses on biomaterials used in the human joint implants [22], which may lead to various bio-tribocorrosion responses and mechanisms. The presence and characteristic of tribofilm depend on the loading conditions and are one of the reasons for various tribocorrosion responses [23]. YAN et al [24] reported that normal load may result in an increase in the corrosion and the metal ion release rate of a CoCrMo alloy implant. On the other hand, STACK et al [25] demonstrated that the rate of bio-tribocorrosion of Co−Cr in the Ringer's solution can be decreased by applying higher normal loads. In another study, MATHEW et al [26] used two different test set-ups and reported that the tribocorrosion behaviour of a low carbon CoCrMo was governed by the normal loads in both set-ups.

According to the literature, in the field of tribocorrosion, there are different acceptable procedures such as mechanistic and synergistic approaches [27]. However, synergistic approach is one of the acceptable methods by which the role of corrosion and wear components on tribocorrosion can quantitatively be determined [28]. Although the bio-tribocorrosion of titanium alloys has been widely investigated, few researches have been carried out to evaluate the effect of applied normal load on the bio-tribocorrosion behaviour. In this study, the synergistic tribocorrosion behaviour of Ti6Al4V was evaluated in phosphate buffered saline solution under various normal loads of 3−30 N. The experiments were carried out according to ASTM G119−09 standard [29] using a ball-on-disk tribometer with in-situ electrochemical measurements.

2 Experimental

The wear−corrosion tests were performed according to ASTM G119−09, which is based on the following equation:

$$T=W_o+C_o+S \tag{1}$$

where T is the total rate of material loss during wear−corrosion, i.e., the tribocorrosion rate, W_o is the pure wear rate in the absence of corrosion (i.e., cathodic protection of specimen during the tribocorrosion test), C_o depicts corrosion rate during stagnant condition, and S is quantitative synergy (synergy rate) that shows the interaction between mechanical and electrochemical damages. To specify the total wear and corrosion rates in the tribocorrosion condition, it is needed to obtain C_W, the total corrosion component of tribocorrosion rate as measured in the presence of wear, and W_C, the total wear component of tribocorrosion rate. C_W can be calculated using Eq. (2), which is based on the Faraday's law [30]:

$$C_W=\frac{kI_{corr}E_W}{v} \tag{2}$$

where k is a constant (1.036×10^{-8} mg/(μA·s)), I_{corr} (μA) is corrosion current which can be achieved by Tafel extrapolation from polarization curves during tribocorrosion, E_W is dimensionless equivalent weight of the material, which is 11.65 for Ti6Al4V in accordance with ASTM G102−99 [30], and v is sliding speed in m/s. W_C is obtained using the following equation:

$$W_C=T-C_W \tag{3}$$

Synergy rate can also be obtained as the sum of ΔC_W (change of corrosion rate arising from wear, i.e., C_W-C_o) and ΔW_C (change of wear rate resulting

from corrosion, i.e., W_C-W_o):

$$S=\Delta C_W+\Delta W_C \quad (4)$$

In the present study, a Ti6Al4V round bar with a diameter of 32 mm was used as the test material. Chemical composition of the alloy was obtained using optical emission spectroscopy (OES) and is presented in Table 1. The bar was sliced into the disks with a thickness of 3 mm. The surface of specimens was then polished to reach an average surface roughness (R_a) of (0.30±0.07) μm.

Table 1 Chemical composition of Ti6Al4V alloy (wt.%)

Al	V	Fe	Mo	Si	Cu
6.37	4.33	0.03	0.01	0.01	0.01
W	Nb	Ni	Sn	Mn	Ti
<0.01	0.008	<0.005	<0.005	<0.004	Bal.

A polymeric cup was mounted on an existing ball-on-disk tribometer for conducting tribo-corrosion and pure wear tests. Figure 1 schematically shows the set-up used for the tribocorrosion test. The tests were conducted in a three-electrode cell at room temperature. The counter and reference electrodes were platinum and saturated Ag/AgCl, respectively. A bronze ring on the rotating shaft in connection with a fixed graphite electrode was used to electrically connect the rotating disk sample with the potentiostat. The experiments were performed in a phosphate buffered saline (PBS) solution. The PBS was prepared in accordance with ASTM F2129−15 [31] with the composition of 8 g/L NaCl, 0.2 g/L KCl, 1.15 g/L Na_2HPO_4 and 0.2 g/L KH_2PO_4 in distillated water.

The wear−corrosion and pure wear tests were conducted under various normal loads of 3, 8, 15 and 30 N (corresponding to the maximum Hertzian contact pressures of 816, 1107, 1395 and 1758 MPa) at a sliding velocity of 0.1 m/s (160 r/min). Under standard walking conditions, hip joint bearings as the severest loading condition normally imposed contact pressures less than 100 MPa [32,33]. However, the contact pressure can significantly increase due to the malpositioning of the bearings such as the head displacement. For example, the head displacement in the range of 0.1−2.0 mm leads to the maximum contact pressure ranging from 850 MPa to 2 GPa [34]. This justifies the selected contact pressures to cover the extreme loading conditions of the hip bearings.

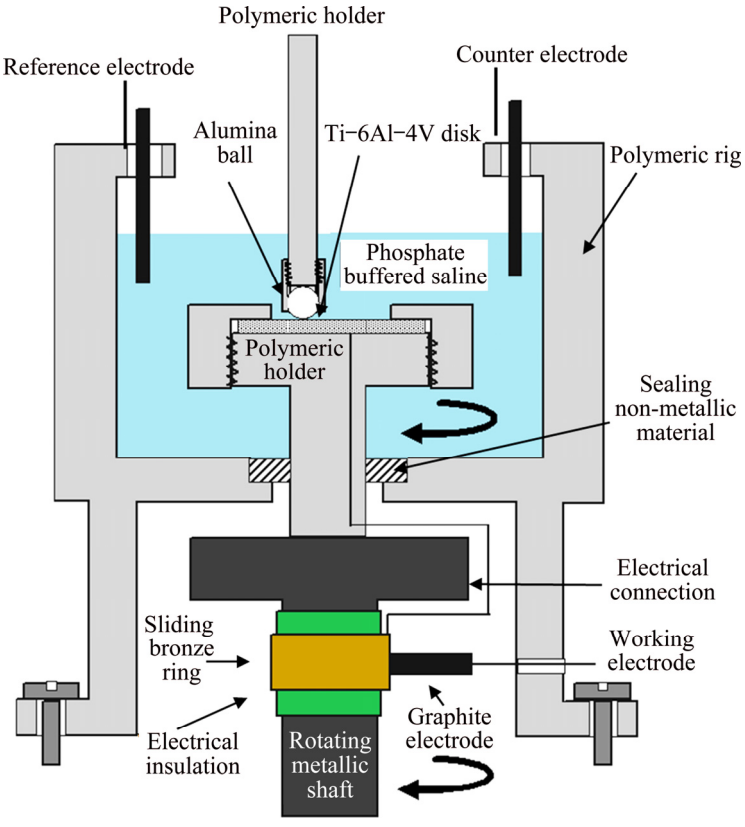

Fig. 1 Schematic tribocorrosion set-up mounted on ball-on-disk tribometer to obtain electrochemical signals

Alumina balls, 5 mm in diameter with a hardness of $HV_{0.1}$ 1550 and surface roughness of about 0.12 μm were used as the counterpart. The nominal chemical composition of the alumina ball was: 48.6 wt.% Al, 46.4 wt.% O and 5.0 wt.% Si. The wear−corrosion tests were performed at open circuit potential (OCP). The pure wear tests (i.e., to measure W_o) were performed under cathodic protection by applying a potential of −1000 mV relative to OCP [29]. Although some investigators have argued that this is not pure wear condition because hydrogen atoms as a product of cathodic reactions can change the wear behaviour of materials in some circumstances [35]; it is still common to refer to the tests under cathodic protection as pure wear tests [36]. The specimens were cleaned with acetone in an ultrasonic bath before and after testing. To obtain the tribocorrosion and pure wear rates, mass losses were measured after a sliding distance of 300 m by weighing the samples with an accuracy of 10^{-4} g using electronic microbalance. Each experiment was repeated three times, and the average material removal rate and standard deviation were reported.

The electrochemical measurements were performed using a 302N Autolab potentiostat/galvanostat and NOVA 1.9 software coupled to the ball-on-disk tribometer. The changes in OCP of the samples versus Ag/AgCl electrode were recorded during the wear−corrosion tests. To obtain the corrosion rate of the samples during tribocorrosion (C_W), a distinct series of the wear-corrosion tests under each condition were run and the polarization tests were conducted after sliding for 5 min using a scan rate of 1 mV/s. The polarization curves were also obtained in the stagnant and flow states, i.e., rotating of the disk without any contact with the ball counterpart. In these conditions, the samples were immersed in the solution for 1 h to stabilize OCP, and the polarization tests were then conducted with a scan rate of 0.167 mV/s (0.6 V/h).

Nano-hardness profile measurement on the cross section of the pure wear and wear−corrosion tracks was carried out by a nano-hardness tester using a Berkovich indenter under a load of 10 mN with loading/unloading rates of 0.2 mN/s. Six indentations were carried out at each depth below the tribocorrosion and pure wear surfaces and the average values were reported. The tribocorrosion and pure wear surfaces were further studied using scanning electron microscopy (SEM), energy dispersive spectroscopy (EDS), and secondary ion mass spectroscopy (SIMS).

3 Results and discussion

3.1 Nano-hardness properties of wear tracks

The nano-indentation test was performed at depths of 1−4 μm by an incremental step of 1 μm on the cross sections of the tribocorrosion and pure wear tracks after sliding under various normal loads of 3−30 N. The load−penetration curves at a depth of 1 μm for the wear tracks obtained under various normal loads in the tribocorrosion and pure wear (i.e., sliding under cathodic protection) conditions are typically shown in Figs. 2(a) and (b), respectively. Figure 2(a) also shows that the penetration depth due to the indentation load consists of two parts of elastic and plastic deformations. The hardness values shown in Fig. 2,

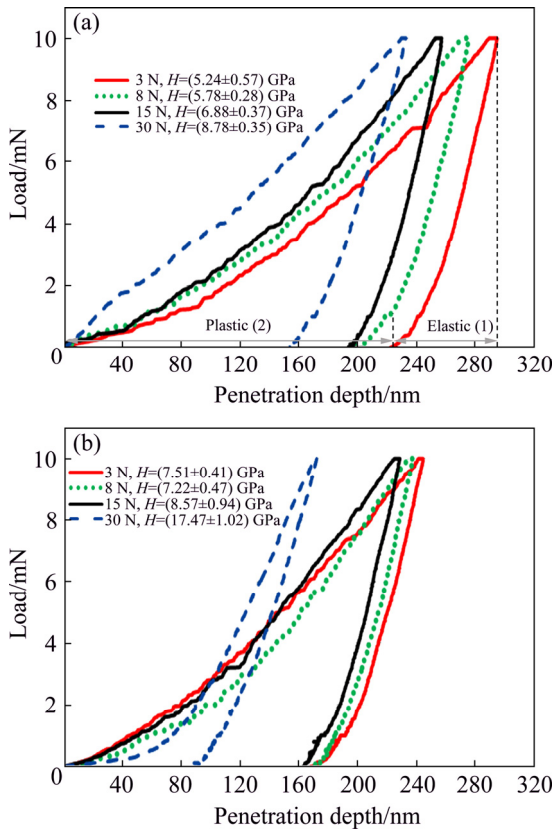

Fig. 2 Variation of nano-indentation load versus penetration depth for Ti6Al4V at depth of 1 μm beneath wear surface following tribocorrosion (a) and pure wear (b) tests under normal loads of 3, 8, 15, and 30 N (Elastic (1) and plastic (2) depths of penetration are typically shown for tribocorrosion sample under normal load of 3 N)

were obtained from the plastic penetration depth [37].

The average hardness (*H*) extracted from the curves [37] such as in Fig. 2 at various depths beneath the wear tracks (1−4 μm) of both pure wear and tribocorrosion samples under normal loads of 3−30 N is presented in Fig. 3. A decrease in hardness was observed as the distance from the wear surface was increased. The higher hardness of the regions just below the wear surface compared with the bulk hardness ((4.9±0.5) GPa) was attributed to the work hardening due to plastic deformation during sliding, which was also reported by other investigators [10,38]. The plastic deformation of the regions below the wear track of the tribocorrosion samples under the normal loads of 3−30 N is shown in Fig. 4. The contact stresses during sliding deformed and aligned the subsurface material towards the frictional direction. The deformation under a normal load of 3 N was probably narrow in depth and not detectable in the SEM image (Fig. 4(a)). As the normal load increased, the depth of deformed region beneath the wear track was increased. For example, the depth of plastic deformation of about 6 μm under a normal load of 8 N (Fig. 4(b)) was increased to 13 μm under a normal load of 30 N (Fig. 4(d)). Under a normal load of 3 N in Fig. 3(a), a hardness close to the bulk hardness of Ti6Al4V ((4.9±0.5) GPa) was obtained at the depths of 3−4 μm. However, as the normal load increased to 30 N, a hardness of about 6.1 GPa was obtained at a depth of 4 μm in Fig. 3(d). This indicated that the material at this depth was highly affected by the contact stresses as shown in Fig. 4(d). The plastic deformation likely occurred in Ti6Al4V by dislocation slip and deformation twins during sliding [39,40]. Intersections between dislocation and twins hindered more plastic deformation during wear, leading to the work hardening [41].

Comparing Figs. 3(a−d) revealed that the near surface hardness increased as the normal load increased for both pure wear and tribocorrosion samples. As the normal load increased, for example, from 3 to 30 N, the average hardness at the depth of 1 μm increased from 7.5 to 17.5 GPa for the pure wear and from 5.2 to 8.8 GPa for the tribocorrosion samples, respectively. An increase in the normal load could provide more plastic deformation and work hardening on the wear surface, resulting in a higher density of dislocations and the formation of other crystal defects such as

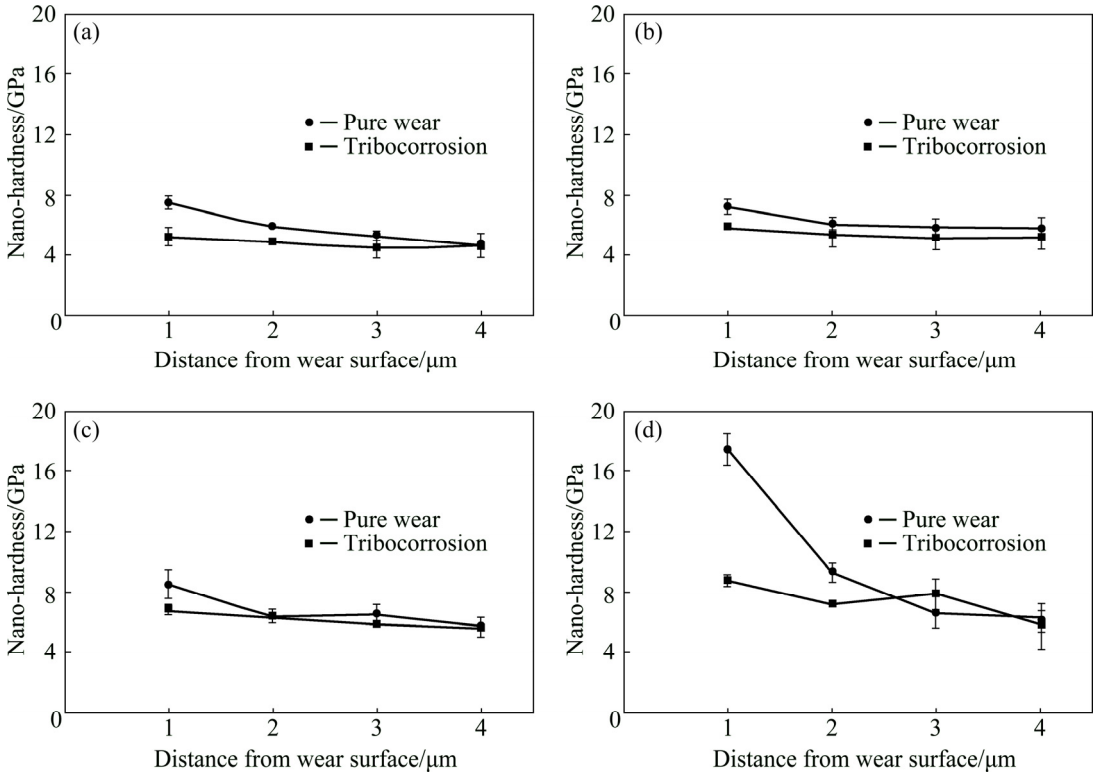

Fig. 3 Nano-hardness profiles of wear samples under normal loads of 3 N (a), 8 N (b), 15 N (c) and 30 N (d) under tribocorrosion and pure wear conditions

twins and voids during wear [42,43]. This led to a higher hardness in the near surface regions under the higher normal loads in Fig. 3.

Figure 3 also showed that the maximum hardness of the subsurface was higher in the pure wear samples as compared with the tribocorrosion samples under various normal loads. The lower hardness of the tribocorrosion subsurface, as compared with pure wear, could be due to the formation of a bio-tribofilm and the removal of work hardened layers exposed to the corrosive medium (PBS, phosphate buffered saline) on the sliding surface during tribocorrosion. The formation of tribofilm, which was only about 100 nm in thickness under a normal load of 30 N [44], could lower the magnitude of tribological stresses in Ti6Al4V substrate. Therefore, a lower plastic deformation and work hardening in the subsurface regions of the tribocorrosion samples resulted in a lower hardness as compared with the pure wear samples in Fig. 3.

Figure 3 showed that the difference between the maximum hardness of pure wear and tribo-corrosion samples was especially considerable under a normal load of 30 N in which the maximum hardness of the pure wear sample reached about HV 1780 (17.5 GPa) at 1 μm away from the surface, which was about twice of that in tribocorrosion sample (HV 900 or 8.8 GPa). The higher hardness of the subsurface region for the pure wear sample under a normal load of 30 N was probably due to high strain and strain rate that occurred during sliding, leading to the formation of a highly severe plastic deformation (SPD) layer [45]. Under the lower normal loads, this SPD region could form much closer to the wear surface than a depth of 1 μm where the hardness measurements were obtained.

3.2 Micrographs of wear tracks

Figure 5 showed back scatter electron SEM images of Ti6Al4V tribocorrosion tracks under various normal loads. The wear tracks showed indications of grooves and micro-abrasion due to sliding against alumina balls. The back scatter electron micrographs in Fig. 5 also represented some darker patches, which could be indicative of the formation of a different phase on the wear surfaces. The EDS analyses of various regions in Fig. 5 are listed in Table 2. According to the analyses in the table, the darker regions contained oxygen and phosphorous as compared with the

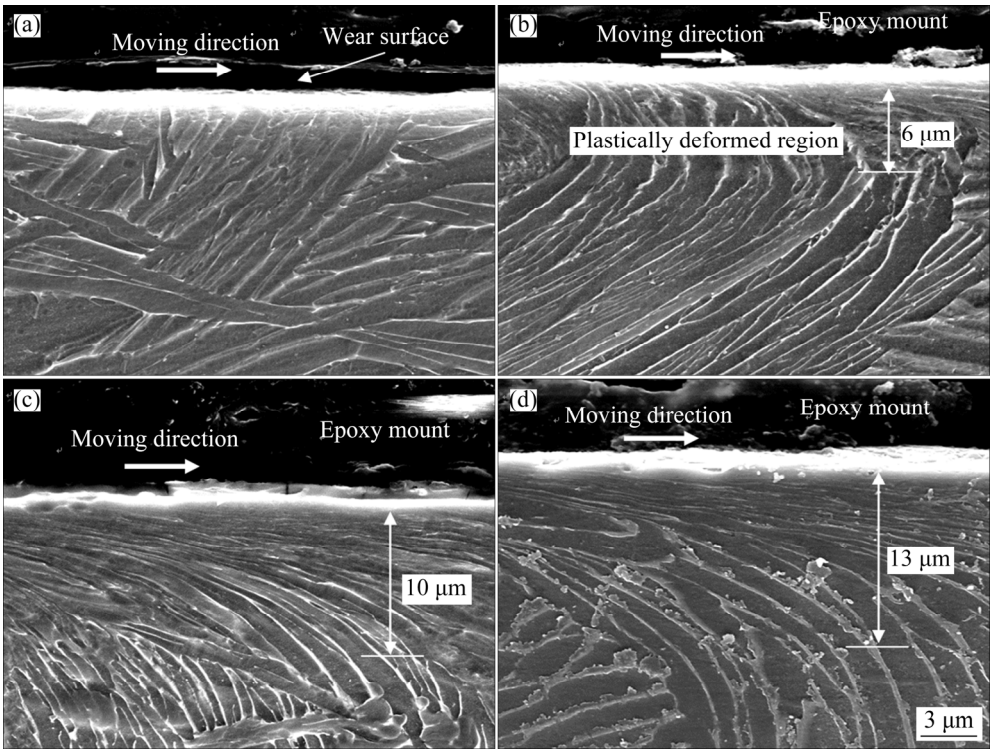

Fig. 4 Subsurface micrographs of tribocorrosion samples after 300 m of sliding under various normal loads of 3 N (a), 8 N (b), 15 N (c) and 30 N (d) (The cross sections were chemically etched with the Kroll's etchant with $V(H_2O):V(HNO_3):V(HF)=92:6:2$)

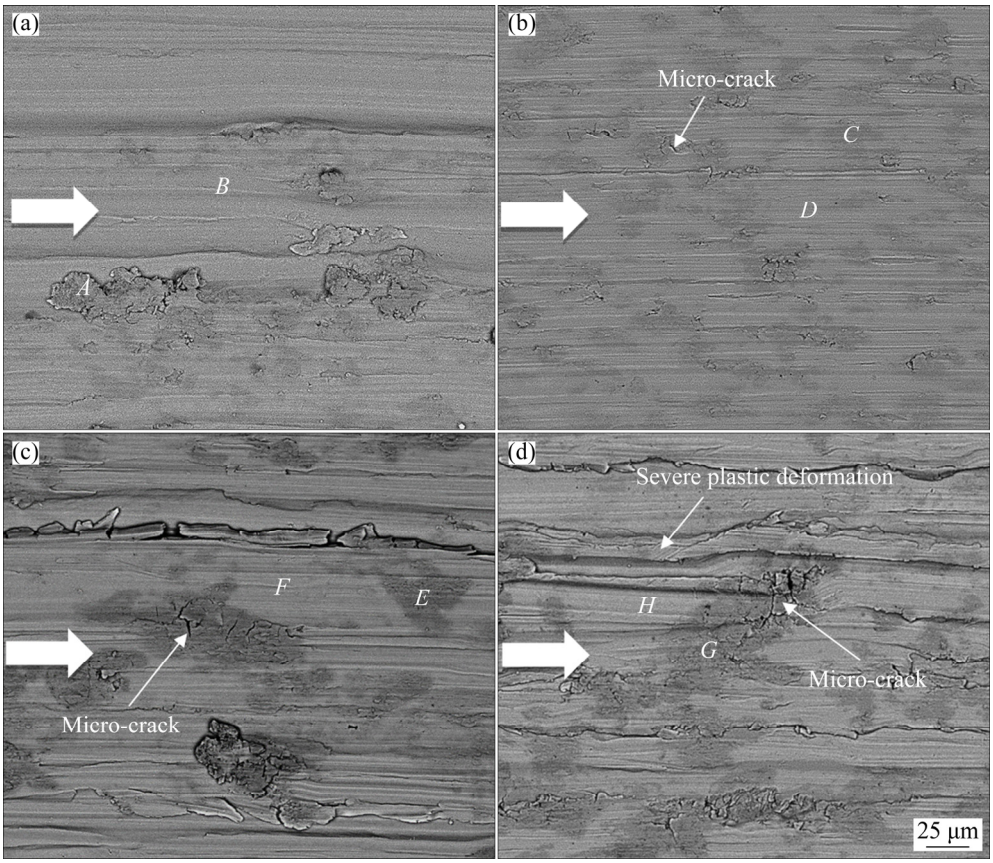

Fig. 5 Back scatter electron SEM images of tribocorrosion tracks under various normal loads of 3 N (a), 8 N (b), 15 N (c) and 30 N (d) in PBS solution after 300 m of sliding (Coarser arrows show the sliding direction)

metallic brighter regions with almost no oxygen and phosphorous. The dark patches indicated the formation of bio-tribofilms due to tribo-mechanical and tribo-chemical reactions during sliding. The oxygen in the solution reacted easily with deformed titanium alloy on the sliding surface, resulting in an oxygen-rich tribofilm [44] during tribocorrosion testing. Table 2 showed that the oxygen content of the dark patches increased with the increase in normal load, which could indicate the formation of thicker bio-tribofilms. The surface coverage of the layers was also increased at the higher normal loads of 15 and 30 N as could be seen in Fig. 5. PERRET et al [46] demonstrated that the tribofilm could act as the obstacles for dislocation annihilation in the free surface. This could suggest larger hardening area due to the higher coverage of the tribofilm under higher normal loads, which in turn could better support the tribofilm during sliding. Under higher normal loads, a more plastic deformation of the wear surface (Fig. 4) resulted in a higher density of dislocations and twins, which led to an increase in the stored energy in the surface and subsurface of the material [47]. The higher stored energy of the surfaces could reduce the activation energy of chemical reactions and enable the surface to react more easily with the solution during tribo-corrosion [48]. Moreover, a subsurface material with higher hardness and strength developed under higher normal loads (Fig. 3) would make a more durable tribo-layer during sliding.

Table 2 EDS results of dark areas (*A*, *C*, *E* and *G*) and bright regions (*B*, *D*, *F* and *H*) on tribocorrosion surfaces shown in Fig. 5

Normal load/N	Region	Content/wt.%				
		Ti	Al	V	O	P
3	*A*	90.2	4.1	1.3	3.3	1.1
	B	91.8	6.5	1.7	−	−
8	*C*	83.3	5.5	2.5	7.4	1.3
	D	92.4	5.3	2.1	0.3	−
15	*E*	80.2	7.3	1.8	9.9	0.8
	F	92.3	6.0	1.8	−	−
30	*G*	77.0	6.7	2.1	11.8	2.4
	H	92.0	5.9	1.9	0.1	0.1

To verify the presence of phosphorous and oxygen in the bio-tribofilms, the tribocorrosion track formed under a normal load of 30 N was analyzed by SIMS (secondary ion mass spectrometry) and the depth profile is presented in Fig. 6. The results revealed that phosphorous and oxygen ions appeared on the wear surface. The phosphorous ions and water in PBS solution could react with bare titanium surface and form some phosphorous-containing complexes [49−51]. HANAWA et al [49] indicated that the repassivated film on titanium in Hanks' solution consisted of TiO_2, $TiO(OH)_2$ and titanium phosphate using X-ray photoelectron spectroscopy and Auger electron spectroscopy. In accordance with the model proposed by HEALY and DUCHEYNE [50], titanium oxide could somewhat dissolve in the physiological body fluid and phosphorous ions are adsorbed in the passive film at the same time. The adsorbed phosphorous ions then reacted with Ti—OH and were incorporated into the passive film. This mechanism needed a long period of time, i.e., more than 5000 h to occur in a stagnant condition [51]. However, the contact stresses during sliding could increase the driving force of the reaction, and result in the formation of phosphorous and titanium complex on the wear surface during tribocorrosion tests [52].

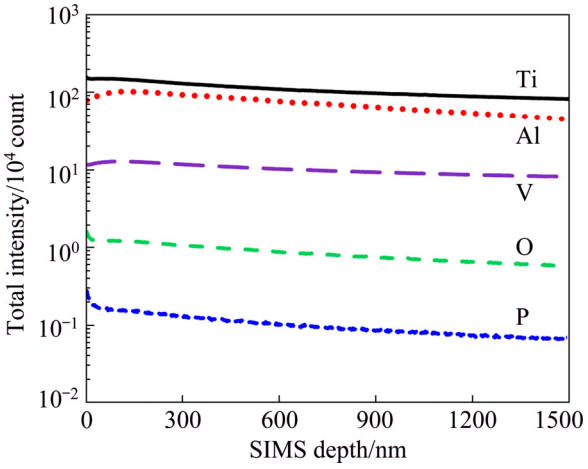

Fig. 6 SIMS depth profiles of tribocorrosion tracks after 300 m of sliding under normal load of 30 N

3.3 Potentiodynamic polarization

The polarization curves of samples during tribocorrosion under various normal loads of 3−30 N are shown in Fig. 7. The polarization curves in the stagnant and flow (i.e., sample rotating in the solution without loading) conditions are also presented in Fig. 7. Figure 7 revealed that at potentials higher than 0.23 V (vs Ag/AgCl), the electrochemical current densities were approximately equal in the stagnant and flow conditions. The anodic branch of polarization curves in these two conditions exhibited a passive plateau at a potential span up to about 1.5 V (vs Ag/AgCl). Figure 7 showed a more negative corrosion potential, for the sample during flow as compared with the stagnant condition. This could be related to the easier removal of the unstable oxides i.e., TiO and Ti_2O_3 [53], from the passive TiO_2 layer in the flow condition. These oxides, which loosely adhered to the passive film [54], were easily removed from the surface during rotation of the disk in the solution and resulted in a lower corrosion potential, i.e., a higher tendency to corrosion.

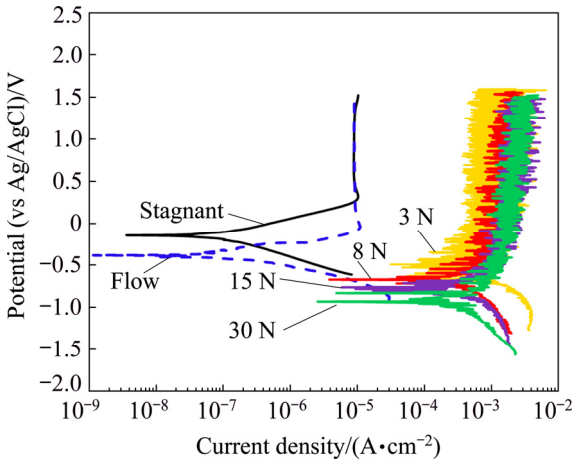

Fig. 7 Polarization curves of samples under stagnant, flow, and tribocorrosion conditions at various normal loads of 3, 8, 15 and 30 N

As compared with the stagnant and flow conditions, the polarization curves were significantly changed during tribocorrosion, i.e., under loading. There were about 345 and 110 mV decrease in the corrosion potential under a normal load of 3 N compared with the stagnant and flow conditions, respectively. This suggested a higher tendency of the alloy for corrosion during tribocorrosion [55], which was probably due to the local removal or destruction of the passive film. The decrease in the corrosion potential of the tribocorrosion samples compared with the stagnant condition was about 527, 639 and 791 mV under normal loads of 8, 15 and 30 N, respectively. The

lower corrosion potential during sliding under higher normal loads was due to the higher plastic deformation of the wear surface (Fig. 4) leading to easier reaction [48] during tribocorrosion.

Figure 7 also showed an increase of about three orders of magnitude in the corrosion current densities (J_{corr}) during the tribocorrosion compared with those in the stagnant and flow conditions. This was also consistent with the study conducted by HACISALIHOGLU et al [56]. During tribocorrosion, the passive film was damaged, resulting in a direct contact between the active bare metal and the corrosive medium, which led to unrestricted charge transfer responses [57] and a sharp increase in the corrosion rate. It could be observed from Fig. 7 that there was no tangible change in corrosion current density under various normal loads. A higher corrosion current density was expected under a higher normal load due to a higher surface damage, a larger real contact area and higher plastic deformation on the surface. However, as the normal load increased from 3 to 30 N, J_{corr} was changed from 270 to 210 μA/cm^2. It seems that the formation of tribofilm with higher coverage on the wear surfaces under the higher normal loads in Fig. 5 could control the corrosion rate by lowering the direct contact of the mating surfaces.

3.4 Open circuit potential and coefficient of friction

The changes in the coefficient of friction and open circuit potential with sliding distance during tribocorrosion under various normal loads are presented in Fig. 8. Prior to loading, the OCP increased in the PBS solution, which was related to the formation and growth of the passive film on Ti6Al4V surfaces [58]. At the onset of sliding, a considerable decrease in the potential was observed. The decrease in OCP or a higher tendency of the alloy for corrosion was attributed to the destruction of the passive film and plastic deformation on the contact regions (Fig. 4), which also resulted in a higher corrosion rate in Fig. 7. The tribocorrosion surface became more active under the higher normal loads, which led to a more negative OCP (Fig. 8).

The film destruction and excessive plastic deformation on asperities, which increased the surface energy, resulted in a more active surface by a sharp drop in the OCP at the start of sliding. In stage A shown in Figs. 8(c) and (d), a small gradual increase in the potential could be observed under normal loads of 15 and 30 N. By the onset of sliding, a nobler surface was formed probably due to the formation of tribofilms as shown in Fig. 5, which allowed the OCP to shift gradually towards

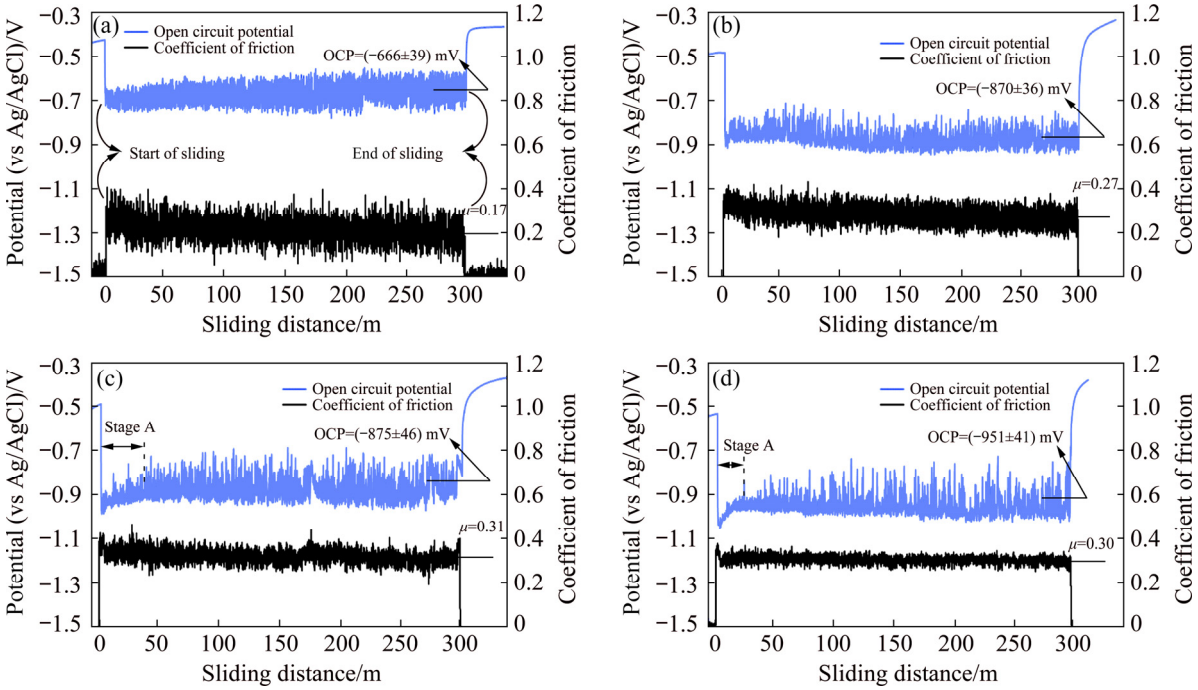

Fig. 8 Coefficient of friction and open circuit potential vs sliding distance of Ti6Al4V alloy under normal loads of 3 N (a), 8 N (b), 15 N (c) and 30 N (d) before, during and after tribocorrosion

the higher potentials. In fact, a transient in the dominant wear mechanism from a mechanical wear to a tribochemical wear could exist at this stage [48].

Figure 8 showed that after the tribocorrosion tests, the OCP increased rapidly and shifted to a nobler potential as a result of the repassivation of the contact areas and the presence of the tribofilms. The fluctuations in the coefficient of friction amplitude were decreased as the applied normal load increased. The existence of the fluctuations in the coefficient of friction could be related to a high adhesion between Ti6Al4V and alumina counterpart, causing a stick//slip [59]. Therefore, a lower fluctuation in the trace of coefficient of friction as the normal load increased was attributed to a lower adhesion due to the formation of a tribofilm with higher surface coverage as depicted in Fig. 5. The tribofilm could also increase the average tangential strength of the sliding interface and, therefore, increase the average coefficient of friction under higher normal loads as shown in Fig. 8. The higher amount of plastic deformation and work hardening under higher normal loads could result in a higher increase in the shear strength than the hardness values of the wear surface and subsurface regions in Fig. 3 [60]. This could also contribute to the increase in the average coefficient of friction with normal load. Figures 8(b−d) showed that there were some instantaneous peaks in the OCP traces towards the anodic side under normal loads of 8, 15 and 30 N, respectively. This meant that some periods with low amplitude fluctuations were observed under the higher normal loads, specially 30 N. The formation of tribofilm patches on the real contact areas during sliding could be responsible for the peaks observed.

3.5 Synergetic tribocorrosion

Figure 9 presents the tribocorrosion (T) and pure wear (W_o) rates of Ti6Al4V in the PBS under various normal loads of 3−30 N. The figure showed that as the normal load increased, the tribocorrosion rate increased as expected according to the Archard's wear equation [61]. However, the specific tribocorrosion rate (STR) as obtained by dividing the tribocorrosion rate by the normal load, which compared the severity of damage with the normal load, showed a different trend in Fig. 9. The figure showed a higher STR and a severer wear under a normal load of 8 N compared those with 3 N. The drop in STR under higher loads of 15 and 30 N indicated that the wear became milder probably due to a higher coverage of the tribofilm (Fig. 5) and the decrease in adhesion between the mating surfaces.

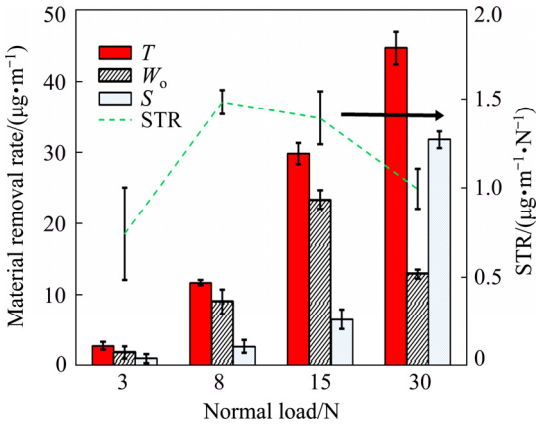

Fig. 9 Tribocorrosion (T), pure wear (W_o), synergy rate (S) and specific tribocorrosion rate (STR) of Ti6Al4V in PBS solution under various normal loads of 3, 8, 15 and 30 N

The pure wear surfaces under various normal loads are presented in Fig. 10. Figures 10(a) and (b) showed grooves and plastic deformation on the pure surfaces under normal loads of 3 and 8 N, similar to the tribocorrosion surfaces in Fig. 5, which resulted from sliding against the hard counterpart, i.e., alumina ball [6]. This could suggest the occurrence of ploughing as a dominant wear mechanism on the pure wear surfaces. In comparison, the presence of oxygen-rich tribofilm on the tribocorrosion surfaces (Fig. 5 and Table 2) in conjunction with the ploughing and plastic deformation indicated that the predominant wear mechanism was a chemical wear accompanying with ploughing.

A remarkable point in Fig. 9 was that increasing the normal load from 15 to 30 N resulted in a decrease of about 45% in the pure wear rate (W_o). A higher work hardening under a higher normal load of 30 N resulted in a subsurface hardness of about two times higher compared with a normal load of 15 N in the pure wear condition during sliding (Figs. 3(c) and (d)). Therefore, considering a twice increase in the normal load, the Archard's wear equation [61] would predict a similar wear rate. However, SEM micrographs of the pure wear surfaces in Fig. 10 under normal loads of 15 and 30 N showed that a larger amount of wear debris was generated under a normal load

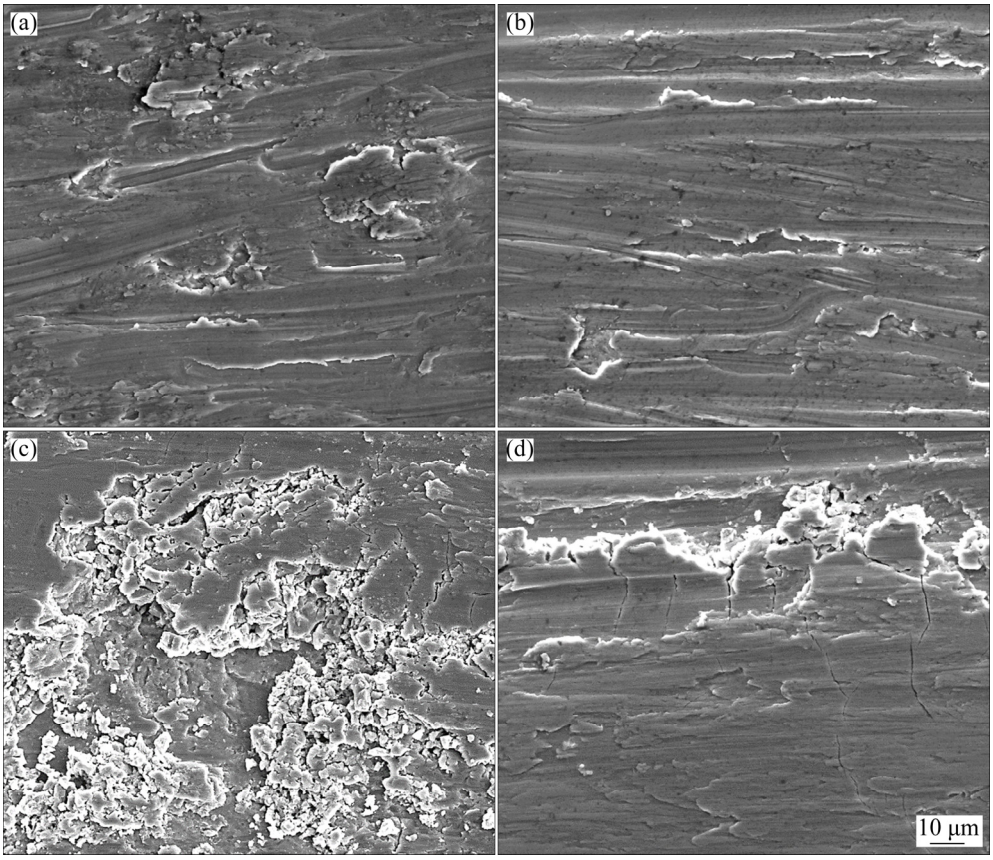

Fig. 10 SEM images of pure wear tracks (i.e., under cathodic protection of −1 V (vs Ag/AgCl) in PBS solution) under normal loads of 3 N (a), 8 N (b), 15 N (c) and 30 N (d) after 300 m of sliding

of 15 N due to the brittle fracture of the material as the predominant wear mechanism. This led to a higher wear coefficient and, therefore, a higher wear rate. Furthermore, according to our previous published paper [44], plastic deformation and work hardening of the wear surface and subsurface during sliding could result in the grain refinement of Ti6Al4V. The grain refinement is a strengthening mechanism, which at the same time, increases the hardness and toughness of the material [62]. Under a normal load of 30 N, a higher plastic deformation led to a higher work hardening and a higher hardness (Fig. 3(d)), which could result in a more grain refinement and a higher toughness of the wear surface and subsurface [44]. This probably led to a change in the wear mechanism from a severer brittle fracture to a more ductile deformation. This caused a lower generation of wear debris resulting in a lower wear coefficient and, therefore, a lower wear rate under a normal load of 30 N as compared with 15 N during pure wear condition.

The synergistic interaction between wear and corrosion was obtained from Eq. (1) and also shown in Fig. 9. The synergy rate (S) was positive under all normal loads. This revealed that the material removal rates were enhanced by the presence of the corrosive medium (PBS), as compared with the pure wear rates. To study the synergistic effect, the tribocorrosion data of Ti6Al4V in PBS using Eqs. (1), (3) and (4) are listed in Table 3. Under various normal loads, W_C, the wear component of the tribocorrosion rate or T (T=W_C+C_W), i.e., the total wear rate in the presence of corrosion, was much higher than C_W, the corrosion component of tribocorrosion rate. The contribution of W_C ranged from 97% to 99.7% under normal loads of 3 to 30 N, respectively. This revealed that the tribocorrosion of Ti6Al4V in PBS was wear-dominant [19,55]; however, the influence of corrosion on the wear rate could not be neglected. Although, C_W comprised a very small portion of tribocorrosion rates (T); a high value of ΔW_C, i.e., the change in wear rate due to corrosion, in Table 3, showed that the wear rate was mainly enhanced due to the presence of corrosion. This was more pronounced under a normal load of 30 N, where the presence of

corrosion unexpectedly enhanced the tribocorrosion rate to more than 245% respect to the pure wear rate as compared with 52%, 30% and 28% under the lower normal loads of 3, 8 and 15 N, respectively. The higher tribocorrosion rate (T) compared with the pure wear rate (W_o) might be related to the higher removal rate of the work hardened layer during tribocorrosion. Figure 3 revealed a lower subsurface hardness for the tribocorrosion compared with the pure wear samples, which was also attributed to the removal of the wok hardened layer. The removal of the work hardened layer in the tribocorrosion tests was due to the destructive interaction between corrosion and mechanical wear. It meant that the formation and subsequent removal of corrosion products on the work harden layer increased the corrosion rate during tribocorrosion, which also resulted in a higher tribocorrosion rate compared with pure wear shown in Fig. 9 and Table 3. The removal of the work harden layer in tribocorrosion condition was the reason for the large increase in the ΔW_C and W_C in Table 3. A higher value of ΔW_C resulted in a higher synergy rate (S=ΔW_C+ΔC_W), leading to a higher tribo-corrosion rate (T) as compared with W_o.

To better show the effect of interaction between wear and corrosion, i.e., the contribution of synergy on the tribocorrosion rate, the S/T ratio was calculated under various normal loads and presented in Table 3. The S/T ratio was 0.71 under a normal load of 30 N, which implied that 71% of the total tribocorrosion rate was related to the interaction between corrosion and wear, as compared with 22%−34% under the lower normal loads. This suggested that the role of corrosion on the wear degradation was largely increased under a normal load of 30 N. In addition, a lower OCP under a normal load of 30 N in Fig. 8 indicated a higher tendency to corrosion, which led to a higher S/T ratio. This could also be due to the dissolution of the work hardened or SPD layer as discussed earlier. The corrosion and subsequent wear of the layer increased the material removal rate, i.e., the tribocorrosion rate, under the normal loads tested. This was more pronounced under a normal load of 30 N, which resulted in a higher work hardening of the wear surface and higher corrosion and a higher S/T ratio. This clearly indicated the higher effect of the dissolution of work hardened layer on the tribocorrosion rate of Ti6Al4V.

4 Conclusions

(1) There was a high increase in the hardness and decrease in wear debris and wear rate of Ti6Al4V disk against alumina ball in PBS solution as the normal load increased from 15 to 30 N during pure wear.

(2) A higher tribocorrosion rate was obtained compared with the pure wear due to the successive formation and removal of the tribofilms, which were more pronounced under the normal loads higher than 3 N.

(3) EDS and SIMS analyses revealed the formation of tribofilms containing oxygen and phosphorous compounds during tribocorrosion. The presence of the tribofilms led to a higher coefficient of friction with a lower fluctuation under normal loads of 8, 15 and 30 N compared with 3 N during tribocorrosion.

(4) The corrosion component of tribocorrosion rate, C_W, was only a small portion of the tribocorrosion rate (T). However, the presence of corrosion led to 28%−245% increase in the wear

Table 3 Tribocorrosion variables of Ti6Al4V in PBS

Normal load/ N	Variable/(μg·m^{-1})								S/T ratio
	T	C_o	W_o	S=T−C_o−W_o	C_W	W_C	ΔC_W	ΔW_C	
3	2.78±0.52	0.001144±0.00032	1.83±0.83	0.95±0.61	0.08±0.01	2.70±0.30	0.08±0.01	0.87±0.51	0.34±0.03
8	11.67±0.34	0.001144±0.00032	9.0±1.73	2.67±0.93	0.02±0.00	11.65±2.34	0.02±0.00	2.65±2.01	0.23±0.03
15	29.83±1.5	0.001144±0.00032	23.33±1.33	6.50±1.4	0.20±0.01	29.63±3.58	0.20±0.01	6.30±2.47	0.22±0.02
30	44.67±2.23	0.001144±0.00032	12.90±0.64	31.77±1.17	0.12±0.02	44.55±6.01	0.12±0.02	31.65±5.79	0.71±0.06

component of tribocorrosion rate (W_C) compared with the pure wear (W_o) under different normal loads.

(5) The ratio of synergy-to-tribocorrosion rate (S/T) was about 71% under a normal load of 30 N compared with 22%−34% under lower normal loads. This revealed the destructive role of corrosion in the tribocorrosion rate under the highest normal loads.

References

[1] NIINOMI M. Recent research and development in titanium alloys for biomedical applications and healthcare goods [J]. Science and Technology of Advanced Materials, 2003, 4(5): 445−454.

[2] GEETHA M, SINGH A K, ASOKAMANI R, GOGIA A K. Ti based biomaterials, the ultimate choice for orthopaedic implants−A review [J]. Progress in Materials Science, 2009, 54(3): 397−425.

[3] YAZDI R, GHASEMI H M, WANG C, NEVILLE A. Bio-corrosion behaviour of oxygen diffusion layer on Ti−6Al−4V during tribocorrosion [J]. Corrosion Science, 2017, 128: 23−32.

[4] LONG M, RACK H J. Titanium alloys in total joint replacement−A materials science perspective [J]. Biomaterials, 1998, 19(18): 1621−1639.

[5] YIN Mei-gui, CAI Zheng-bing, LI Zheng-yang, ZHOU Zhong-rong, WANG Wen-jian, HE Wei-feng. Improving impact wear resistance of Ti−6Al−4V alloy treated by laser shock peening [J]. Transactions of Nonferrous Metals Society of China, 2019, 29(7): 1439−1448.

[6] YAZDI R, GHASEMI H M, ABEDINI M, WANG C, NEVILLE A. Oxygen diffusion layer on Ti−6Al−4V alloy: Scratch and dry wear resistance [J]. Tribology Letters, 2019, 67(4): 1−15.

[7] ESTHER I, DINAHARAN I, MURUGAN N. Microstructure and wear characterization of AA2124/4wt.%B_4C nano-composite coating on Ti−6Al−4V alloy using friction surfacing [J]. Transactions of Nonferrous Metals Society of China, 2019, 29(6): 1263−1274.

[8] MISCHLER S. Triboelectrochemical techniques and interpretation methods in tribocorrosion: A comparative evaluation [J]. Tribology International 2008, 41(7): 573−583.

[9] MATHEW M T, SRINIVASA PAI P, POURZAL R, FISCHER A, WIMMER M A. Significance of tribocorrosion in biomedical applications: Overview and current status [J]. Advances in Tribology, 2009, 2009: 1−12.

[10] KHAYATAN N, GHASEMI H M, ABEDINI M. Synergistic erosion−corrosion behavior of commercially pure titanium at various impingement angles [J]. Wear, 2017, 380−381: 154−162.

[11] DIOMIDIS N, MISCHLER S, MORE N S, ROY M. Tribo-electrochemical characterization of metallic biomaterials for total joint replacement [J]. Acta Biomaterialia, 2012, 8(2): 852−859.

[12] TAKAKUBO Y, BERCE A, TREBSE R, TAMAKI Y, MILOSEV I, AL-SAMADI A, TIAINEN V M, KONTTINEN Y T. Wear and corrosion in the loosening of total joint replacements (TJRs) [C]//Bio-tribocorrosion in Biomaterials and Medical Implants. Oxford: Woodhead Publishing Limited, 2013: 74−110.

[13] RYU J J, HROTRIYA P S. Synergistic mechanisms of bio-tribocorrosion in medical implants [C]//Biotribo-corrosion in Biomaterials and Medical Implants. Oxford: Woodhead Publishing Limited, 2013: 25−44.

[14] ABEDINI M, GHASEMI H M. Erosion and erosion–corrosion of Al-brass alloy: Effects of jet velocity, sand concentration and impingement angle on surface roughness [J]. Transactions of Nonferrous Metals Society of China, 2017, 27(11): 2371−2380.

[15] CHEN Q Z, THOUAS G A. Metallic implant biomaterials [J]. Materials Science and Engineering R: Reports, 2015, 87: 1−57.

[16] CUI Wen-fang, NIU Feng-juan, TAN Yun-ling, QIN Gao-wu. Microstructure and tribocorrosion performance of nanocrystalline TiN graded coating on biomedical titanium alloy [J]. Transactions of Nonferrous Metals Society of China, 2019, 29(5): 1026−1035.

[17] SAKURAI H. Vanadium distribution in rats and DNA cleavage by vanadyl complex: Implication for vanadium toxicity and biological effects [J]. Environmental Health Perspectives, 1994, 102: 35−36.

[18] RUNA M J, MATHEW M T, ROCHA L A. Tribocorrosion response of the Ti6Al4V alloys commonly used in femoral stems [J]. Tribology International, 2013, 68: 85−93.

[19] LICAUSI M P, IGUAL MUÑOZ A, AMIGÓ BORRÁS V, ESPALLARGAS N. Tribocorrosion mechanisms of Ti6Al4V in artificial saliva by zero-resistance ammetry (ZRA) technique [J]. Journal of Bio- and Tribo-Corrosion, 2015, 1(8): 1−11.

[20] LICAUSI M P, IGUAL MUÑOZ A, AMIGÓ BORRÁS V. Tribocorrosion mechanisms of Ti6Al4V biomedical alloys in artificial saliva with different pHs [J]. Journal of Physics D: Applied Physics, 2013, 46(40): 404003.

[21] LICAUSI M P, IGUAL MUÑOZ A, AMIGÓ BORRÁS V. Influence of the fabrication process and fluoride content on the tribocorrosion behaviour of Ti6Al4V biomedical alloy in artificial saliva [J]. Journal of the Mechanical Behavior of Biomedical Materials, 2013, 20: 137−148.

[22] MANIVASAGAM G, DHINASEKARAN D, RAJA-MANICKAM A. Biomedical implants: Corrosion and its prevention−A review [J]. Recent Patents on Corrosion Science, 2010, 2: 40−54.

[23] WIMMER M A, LAURENT M P, MATHEW M T, NAGAELLI C, LIAO Y, MARKS L D, JACOBS J J, FISCHER A. The effect of contact load on CoCrMo wear and the formation and retention of tribofilms [J]. Wear, 2015, 333: 643−649.

[24] YAN Y, NEVILLE A, DOWSON D. Biotribocorrosion—An appraisal of the time dependence of wear and corrosion interactions: II. Surface analysis [J]. Journal of Physics D: Applied Physics, 2006, 39(15): 3206−3212.

[25] STACK M M, RODLING J, MATHEW M T, JAWAN H, HUANG W, PARK G, HODGE C. Micro-abrasion-corrosion of a Co−Cr/UHMWPE couple in Ringer's solution: An

approach to construction of mechanism and synergism maps for application to bio-implants [J]. Wear, 2010, 269(5−6): 376−382.

[26] MATHEW M T, RUNA M J, LAURENT M, JACOBS J J, ROCHA L A, WIMMER M A. Tribocorrosion behavior of CoCrMo alloy for hip prosthesis as a function of loads: A comparison between two testing systems [J]. Wear, 2011, 271(9−10): 1210−1219.

[27] MATHEW M T, WIMMER M A. Tribocorrosion of passive metals and coatings [M]. Oxford: Woodhead Publishing Limited, 2011.

[28] LÓPEZ A, BAYÓN R, PAGANO F, IGARTUA A, ARREDONDO A, ARANA J L, GONZÁLEZ J J. Tribocorrosion behaviour of mooring high strength low alloy steels in synthetic seawater [J]. Wear, 2015, 338−339: 1−10.

[29] ASTM G119—09. Standard guide for determining synergism between wear and corrosion [S]. Vol. 93. West Conshohocken: ASTM international, 2009.

[30] ASTM G102—99. Standard practice for calculation of corrosion rates and related information [S]. Vol. 89. West Conshohocken: ASTM International, 1999.

[31] ASTM F2129−15. Standard test method for conducting cyclic potentiodynamic polarization measurements to determine the corrosion susceptibility of small implant [S]. Vol. 86. West Conshohocken: ASTM International, 2015.

[32] LIU F, UDOFIA I J, JIN Z M, HIRT F, RIEKER C, ROBERTS P, GRIGORIS P. Comparison of contact mechanics between a total hip replacement and a hip resurfacing with a metal-on-metal articulation [J]. Journal of Mechanical Engineering Science, 2005, 219(7): 727−232.

[33] HODGE W A, CARLSON K L, FIJAN R S, BURGESS R G, RILEY P O, HARRIS W H, MANNA R W. Contact pressures from an instrumented hip endoprosthesis [J]. Journal of Bone and Joint Surgery−Series A, 1989, 71(9): 1378−1386.

[34] LIU F, WILLIAMS S, FISHER J. Effect of microseparation on contact mechanics in metal-on-metal hip replacements−A finite element analysis [J]. Journal of Biomedical Materials Research—Part B: Applied Biomaterials, 2015, 103(6): 1312−1319.

[35] ESPALLARGAS N, MISCHELER S. Tribocorrosion behaviour of overlay welded Ni−Cr 625 alloy in sulphuric and nitric acids: Electrochemical and chemical effects [J]. Tribology International, 2010, 43(7): 1209−1217.

[36] DONG Min-peng, ZHU Ye-biao, WANG Chun-ting, SHAN Lei, LI Jin-long. Structure and tribocorrosion properties of duplex treatment coatings of TiSiCN/nitride on Ti6Al4V alloy [J]. Ceramics International, 2019, 45(9): 12461−12468.

[37] FISCHER C A C. Nanoindentation [M]. 3rd ed. London: Springer Science & Business Media, 2011.

[38] MOHAMMADI F, LUO J L. Effect of cold work on erosion−corrosion of 304 stainless steel [J]. Corrosion Science, 2011, 53(2): 549−556.

[39] WANG Qing-qing, LIU Zhan-qiang. Plastic deformation induced nano-scale twins in Ti−6Al−4V machined surface with high speed machining [J]. Materials Science and Engineering A, 2016, 675: 271−279.

[40] RAVI SHNAKAR M, RAO B C, LEE S, CHAND-RASEKAR S, KING A H, COMPTON W D. Severe plastic deformation (SPD) of titanium at near-ambient temperature [J]. Acta Materialia, 2006, 54(14): 3691−3700.

[41] SALEM A A, KALIDINDI S R, DOHERTY R D, SEMIATIN S L. Strain hardening due to deformation twinning in alpha-titanium: Mechanisms [J]. Metallurgical and Materials Transactions A, 2006, 37: 259−268.

[42] ALPAS A T, HU H, ZHANG J. Plastic deformation and damage accumulation below the worn surfaces [J]. Wear, 1993, 162−164: 188−195.

[43] RIGNEY D A, GLAESER W A. The significance of near surface microstructure in the wear process [J]. Wear, 1978, 46: 241−250.

[44] YAZDI R, GHASEMI H M, ABEDINI M, WANG C, NEVILLE A. Mechanism of tribofilm formation on Ti6Al4V oxygen diffusion layer in a simulated body fluid [J]. Journal of the Mechanical Behavior of Biomedical Materials, 2018, 77: 660−670.

[45] SATO H, MURASE T, FUJII T, ONAKA S, WATANABE Y, KATO M. Formation of a wear-induced layer with nanocrystalline structure in Al−Al_3Ti functionally graded material [J]. Acta Materialia, 2008, 56(17): 4549−5458.

[46] PERRET J, BOEHM-COURJAULT E, CANTONI M, MISCHLER S, BEAUDOUIN A, CHITTY W, VERNOT J P. EBSD, SEM and FIB characterisation of subsurface deformation during tribocorrosion of stainless steel in sulphuric acid [J]. Wear, 2010, 269: 383−393.

[47] HAJIZADEH K, GHOBADI ALAMDARI S, EGHBALI B. Stored energy and recrystallization kinetics of ultrafine grained titanium processed by severe plastic deformation [J]. Physica B, 2013, 417: 33−38.

[48] XU J G, KATO K. Formation of tribochemical layer of ceramics sliding in water and its role for low friction [J]. Wear, 2000, 245(1−2): 61−75.

[49] HANAWA T, ASAMI K, ASAOKA K. Repassivation of titanium and surface oxide film regeneration in simulated bioliquid [J]. Journal of Biomedical Materials Research, 1998, 40: 530−538.

[50] HEALY K E, DUCHEYNE P. The mechanisms of passive dissolution of titanium in a model physiological environment [J]. Journal of Biomedical Materials Research, 1992, 26(3): 319−338.

[51] HEALY K E, DUCHEYNE P. Hydration and preferential molecular adsorption on titanium in vitro [J]. Biomaterials, 1992, 13(8): 553−561.

[52] CZICHOS H. Tribology: A systems approach to the science and technology of friction lubrication and wear [M]. Amsterdam: Elsevier, 1978.

[53] POHRELYUK I M, FEDIRKO V M, TKACHUK O V, PROSKURNYAK R V. Corrosion resistance of Ti−6Al−4V alloy with nitride coatings in Ringer's solution [J]. Corrosion Science, 2013, 66: 392−398.

[54] RAMIRES I, GUASTALDI A C. Study of Ti−6Al−4V biomaterial using electrochemistry and XPS techniques [J]. Quimica Nova, 2002, 25(1): 10−14.

[55] CHEN Jun, ZHANG Qing, LI Quan-an, FU San-ling, WANG Jian-zhang. Corrosion and tribocorrosion behaviors of AISI 316 stainless steel and Ti6Al4V alloys in artificial seawater [J]. Transactions of Nonferrous Metals Society of China, 2014, 24(4):1022−1031.

[56] HACISALIHOGLU I, SAMANCIOGLU A, YILDIZ F, PURCEK G, ALSARAN A. Tribocorrosion properties of different type titanium alloys in simulated body fluid [J]. Wear, 2014, 332−333: 1−8.
[57] SADIQ K, BLACK R A, STACK M M. Bio-tribocorrosion mechanisms in orthopaedic devices: Mapping the micro-abrasion-corrosion behaviour of a simulated CoCrMo hip replacement in calf serum solution [J]. Wear, 2014, 316: 58−69.
[58] GONZÁLEZJ E G, MIRZA-ROSCA J C. Study of the corrosion behavior of titanium and some of its alloys for biomedical and dental implant applications [J]. Journal of Electroanalytical Chemistry, 1999, 471(2): 109−115.
[59] ABEDINI M, GHASEMI H M, NILI AHMADABADI M. Tribological behavior of NiTi alloy against 52100 steel and WC at elevated temperatures [J]. Materials Characterization, 2010, 61(7): 689−695.
[60] HUTCHINGS I. Tribology: Friction and wear of engineering materials [M]. London: Butterworth−Heinemann, 1992.
[61] ARCHARD J F. Contact and rubbing of flat surfaces [J]. Journal of Applied Physics, 1953, 24(8): 981−988.
[62] SURYANARAYANA C. Nanocrystalline materials [J]. International Materials Reviews, 1995, 40(2): 41−64.

磷酸盐缓冲液中 Ti6Al4V 合金在不同法向载荷下的摩擦腐蚀行为

R. YAZDI[1], H. M. GHASEMI[1], M. ABEDINI[2], C. WANG[3], A. NEVILLE[3]

1. School of Metallurgy and Materials Engineering, College of Engineering, University of Tehran, Tehran, Iran;
2. Department of Metallurgy and Materials Engineering, Faculty of Engineering, University of Kashan, Kashan, Iran;
3. Institute of Functional Surfaces, School of Mechanical Engineering, University of Leeds, Leeds, LS2 9JT, UK

摘　要：使用球对盘式摩擦计，在法向载荷为 3~30 N(对应最大赫兹接触压力为 816~1758 MPa)的条件下，研究 Ti6Al4V 合金在磷酸盐缓冲液中对磨氧化铝的摩擦腐蚀行为。纳米硬度测试结果表明，在纯磨损和摩擦腐蚀表面形成加工硬化层。在纯磨损过程中，当法向载荷从 15 N 增加到 30 N 时，表面硬度提高约 100%；然而，当法向载荷为 30 N 时，产生的磨屑越少，磨损率越低。在不同法向载荷下，腐蚀的存在使磨损率增加 28%~245%。与静态相比，在摩擦腐蚀过程中，极化曲线获得的腐蚀电流密度增加 3 个数量级，且开路电位(OCP)向负电位方向偏移。由氧和磷化合物组成的摩擦膜不断形成和消除，使 OCP 曲线达到峰值，并使法向载荷高于 3 N 时的摩擦因数波动减小。

关键词：Ti6Al4V 合金；摩擦腐蚀；纳米硬度；磨损；腐蚀

(Edited by Wei-ping CHEN)